

Breakdown of the Isobaric Multiplet Mass Equation for the $A = 20$ and 21 Multiplets

A. T. Gallant,^{1,2,*} M. Brodeur,³ C. Andreoiu,⁴ A. Bader,^{1,5} A. Chaudhuri,^{1,‡} U. Chowdhury,^{1,6} A. Grossheim,¹ R. Klawitter,^{1,7} A. A. Kwiatkowski,¹ K. G. Leach,^{1,4} A. Lennarz,^{1,8} T. D. Macdonald,^{1,2} B. E. Schultz,¹ J. Lassen,^{1,6} H. Heggen,¹ S. Raeder,¹ A. Teigelhöfer,^{1,6} B. A. Brown,⁹ A. Magilligan,¹⁰ J. D. Holt,^{11,12,9,†} J. Menéndez,^{11,12} J. Simonis,^{11,12} A. Schwenk,^{12,11} and J. Dilling^{1,2}

¹TRIUMF, 4004 Wesbrook Mall, Vancouver, British Columbia, V6T 2A3 Canada

²Department of Physics and Astronomy, University of British Columbia, Vancouver, British Columbia, V6T 1Z1 Canada

³Department of Physics, University of Notre Dame, Notre Dame, Indiana 46556, USA

⁴Department of Chemistry, Simon Fraser University, Burnaby, British Columbia, V5A 1S6 Canada

⁵École des Mines de Nantes, La Chantrerie, 4, rue Alfred Kastler, B.P. 20722, F-44307 Nantes Cedex 3, France

⁶Department of Physics and Astronomy, University of Manitoba, Winnipeg, Manitoba, R3T 2N2 Canada

⁷Max-Planck-Institut für Kernphysik, Saupfercheckweg 1, D-69117 Heidelberg, Germany

⁸Institut für Kernphysik, Westfälische Wilhelms-Universität, D-48149 Münster, Germany

⁹Department of Physics and Astronomy and National Superconducting Cyclotron Laboratory, Michigan State University, East Lansing, Michigan 48824-1321, USA

¹⁰Department of Physics, Florida State University, Tallahassee, Florida 32306, USA

¹¹Institut für Kernphysik, Technische Universität Darmstadt, 64289 Darmstadt, Germany

¹²ExtreMe Matter Institute EMMI, GSI Helmholtzzentrum für Schwerionenforschung GmbH, 64291 Darmstadt, Germany

(Received 27 November 2013; published 19 August 2014)

Using the Penning trap mass spectrometer TITAN, we performed the first direct mass measurements of $^{20,21}\text{Mg}$, isotopes that are the most proton-rich members of the $A = 20$ and $A = 21$ isospin multiplets. These measurements were possible through the use of a unique ion-guide laser ion source, a development that suppressed isobaric contamination by 6 orders of magnitude. Compared to the latest atomic mass evaluation, we find that the mass of ^{21}Mg is in good agreement but that the mass of ^{20}Mg deviates by 3σ . These measurements reduce the uncertainties in the masses of $^{20,21}\text{Mg}$ by 15 and 22 times, respectively, resulting in a significant departure from the expected behavior of the isobaric multiplet mass equation in both the $A = 20$ and $A = 21$ multiplets. This presents a challenge to shell model calculations using either the isospin nonconserving universal sd USDA and USDB Hamiltonians or isospin nonconserving interactions based on chiral two- and three-nucleon forces.

DOI: 10.1103/PhysRevLett.113.082501

PACS numbers: 21.10.Dr, 21.10.Hw, 27.30.+t

The wealth of data obtained from experiments on increasingly exotic nuclei is only possible because of improved radioactive beam production and delivery [1]. Experiments with these improved beams continually challenge existing theories, a challenge often led by precision mass measurements [2]. High-precision atomic mass measurements are crucial in refining nucleosynthesis abundance calculations [3,4], in deepening our understanding of fundamental aspects of the strong force [5–8], pointing to nuclear structure change [9], and providing signatures of exotic phenomena such as nuclear halo formation [9]. A tool from theory currently confronted by increasingly precise mass values is the isobaric multiplet mass equation (IMME) [10], which relates the mass excesses (ME) of isospin multiplet members as

$$\text{ME}(A, T, T_z) = a(A, T) + b(A, T)T_z + c(A, T)T_z^2, \quad (1)$$

where A and T are the mass number and total isospin of the multiplet, and a , b , c are coefficients that depend on all quantum numbers except T_z . In the isospin description of

nucleons, the proton and neutron belong to a $T = 1/2$ doublet with projections $T_z(n) = 1/2$ and $T_z(p) = -1/2$. However, isospin is only an approximate symmetry, broken by electromagnetic interactions and the up and down quark mass difference in QCD. One can see large deviations from the IMME in the $A = 9$ $J^\pi = 3/2^-$ and $A = 33$ and 35 $J^\pi = 3/2^+$ quartets [11–13], and in the $A = 8$ and 32 [14–16] quintets. Suggested explanations for these deviations include isospin mixing and second-order Coulomb effects, requiring cubic dT_z^3 or quartic eT_z^4 terms to be considered.

Many tests of the IMME on proton-rich systems are hindered by a long-standing problem: excessive in-beam contamination. Substantial isobaric background from alkalis and lanthanides often prevents ground-state measurements of exotic nuclei, especially for nuclei produced at low rates. This applies even for beams produced using element-selective laser ionization in a classical hot-cavity resonant ionization laser ion source. We have developed a novel technology for on-line laser ion sources that suppresses any background contamination, enabling a substantial number of

experiments to proceed. This new ion-guide laser ion source (IG-LIS) has allowed the first direct mass measurements of the most proton-rich members of the $A = 20$ and 21 isospin multiplets. Being the lightest isospin multiplets where all members are stable against particle emission, and the lightest isospin multiplets which can be described within the $d_{5/2}$, $s_{1/2}$, and $d_{3/2}$ orbitals (sd shell), the $A = 20$ and 21 multiplets provide an excellent test of the IMME. This can be done experimentally by high-precision mass measurements of $^{20,21}\text{Mg}$ and theoretically by shell model calculations using either the universal sd USDA and USDB isospin nonconserving (INC) Hamiltonian or interactions based on chiral effective field theory.

In a Penning trap, contaminants can be effectively removed if their ratio to the ions of interest remains $\lesssim 100:1$. It is possible to clean beams with higher levels of contamination using either gas-filled Penning traps [17] or multireflection time-of-flight devices [18,19], but these methods suffer from increased preparation times and transport losses. An alternative method is to suppress contamination from surface-ionized species at the source through the use of an IG-LIS. The IG-LIS is conceptually similar to the originally proposed ion-source trap [20,21]; however, it is much simpler because no trap is formed and no buffer gas is used. Figure 1 shows a diagram of the IG-LIS. The isotope production target is typically operated at temperatures above 1900 K. The target production volume is coupled via a heated transfer tube to a positively biased radio-frequency quadrupole (RFQ) ion guide. A repeller electrode [20,22] reflects surface-ionized species, preventing them from entering the ion-guide volume. Neutral particles drift into the ion-guide volume, where element-selective resonant laser excitation and ionization creates an isobar free ion beam. A square-wave RF field radially confines the laser ionized beam. The ion beam is then extracted from the IG-LIS for subsequent mass separation and delivery to the experiment. A complete description of the IG-LIS can be found in Ref. [22].

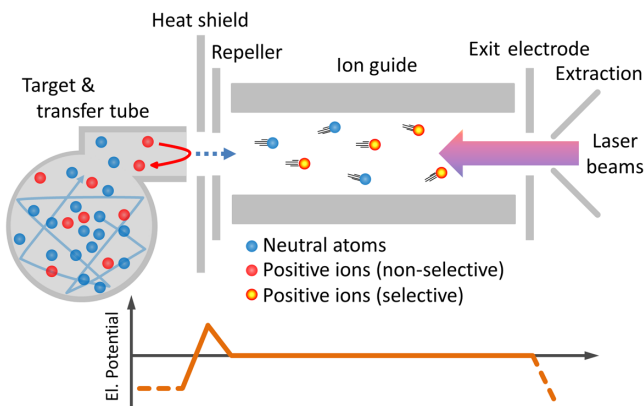


FIG. 1 (color online). A schematic drawing of the ISAC target with the IG-LIS. See the text for a detailed description.

The IG-LIS concept has been implemented and used online for the first time at TRIUMF's isotope separator and accelerator (ISAC) facility. Beams of $^{20,21}\text{Mg}$ were produced by bombarding a SiC target with $40 \mu\text{A}$ of 480 MeV protons. Compared to previous SiC targets, we found that the IG-LIS decreased the magnesium yield by 50 times and the sodium background by 10^6 times. This is a signal-to-background improvement of better than 10^4 .

The TITAN system [23] currently consists of three ion traps: an RFQ cooler and buncher [24], an electron beam ion trap [25] for charge breeding and in-trap decay spectroscopy, and a measurement Penning trap [26] to precisely determine atomic masses. We bypassed the electron beam ion trap because the required precision could be reached without charge breeding. In the measurement Penning trap the mass is determined by measuring an ion's cyclotron frequency ($\nu_c = qB/(2\pi m)$) via the time-of-flight ion cyclotron resonance technique [27]. A typical resonance for ^{21}Mg is shown in Fig. 2. To eliminate any dependence on the magnetic field the ratio of cyclotron frequencies $r = \nu_{c,\text{ref}}/\nu_c$ is taken between a well-known reference and the ion of interest. The reference ion used was ^{23}Na . Because the magnetic field fluctuates in time, due to field decays and temperature or pressure variations, it must be monitored. This monitoring is achieved by performing a reference measurement before and after a measurement of the ion of interest and linearly interpolating to the time when the frequency of the ion of interest was measured. To further limit these fluctuations, the length of a measurement was limited to approximately 1 h. The atomic mass of the nuclide of interest is then calculated from

$$M = r(M_{\text{ref}} - m_e) + m_e, \quad (2)$$

where M is the atomic mass of a nuclide, m_e is the electron mass, and we neglect electron binding energies. Although no contaminants were observed during the measurements, to be conservative we performed a "count class" analysis to account for ion-ion interactions. In the case of ^{20}Mg , the

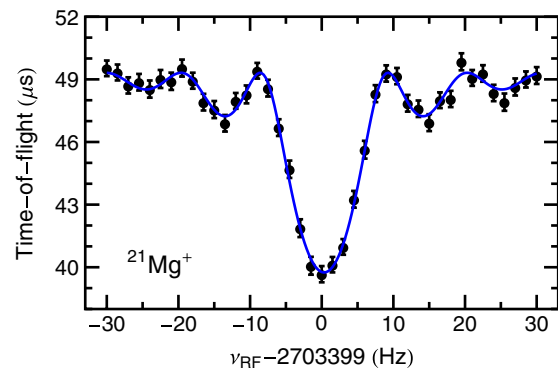


FIG. 2 (color online). Time-of-flight ion cyclotron resonance of $^{21}\text{Mg}^+$ with 97 ms excitation time. The line is a fit of the theoretical shape [27].

TABLE I. Half-lives, number of measurements N , detected number of ions N_{ions} , excitation times T_{RF} , measured frequency ratios and derived mass excesses of $^{20,21}\text{Mg}$. For the frequency ratios, the first two numbers in parentheses are the statistical and systematic uncertainties, while the number in brackets is the total uncertainty; otherwise the quoted uncertainty is the total uncertainty. Half-lives are from the NNDC [31].

Nuclide	$T_{1/2}$ (ms)	N	N_{ions}	T_{RF} (ms)	Frequency ratio r	ME (keV)	ME _{AME2012} (keV)
^{20}Mg	90 (6)	6	1401	97	0.870 765 248 (77) (40) [87]	17 477.7 (18)	17 559 (27)
^{21}Mg	122 (2)	5	31 369	97	0.913 956 913 (33) (9) [35]	10 903.85 (74)	10 914 (16)

statistics were too low (≈ 50 ions/s) for such an analysis. Instead, we follow the procedure in Ref. [28], where the difference between the frequency ratio taken with one detected ion and the ratio with all detected ions was added as a systematic. We also include the conservative mass dependent shift given in Ref. [29], which in the cases here amounts to ≈ 10 ppb. Table I summarizes the measurement results. Our mass excess of 10 903.85 (74) keV for ^{21}Mg agrees well with the tabulated value from AME2012 [30]. The mass excess of 17 477.7 (18) keV for ^{20}Mg deviates by 81 keV as compared to the AME2012, which is a shift of 3σ . In both cases the precision was increased by more than 1 order of magnitude.

Determining the energy level of an isospin multiplet member relies on knowing both the ground-state and excited-state energies accurately. For different experimental techniques, the measured excitation energy depends on separation energies, which can change with improved mass measurements. New mass measurements of the ground states of ^{20}Na [32] and ^{19}Ne [33] led to an improved proton separation energy value for ^{20}Na of 2190.1(11) keV. This value is required to derive the excitation energy of the $J^\pi = 0^+$, $T = 2$ state in ^{20}Na . Combining a new measurement of the excitation energy [34] with the value compiled in [32], an averaged value of 6524.0(98) keV is obtained, a result that is shifted by 10 keV relative to the tabulated value [31]. In ^{21}Mg , a new measurement of the $J^\pi = 1/2^+$ state was completed [35], which, when averaged with the National Nuclear Data Center (NNDC) [36] value, yields 200.5(28) keV. Both of these new values are included in the following analysis.

Table II summarizes the fit results of the quadratic, and higher order forms of the IMME for the $A = 20$ and 21 multiplets. For each multiplet the χ^2 of the fit greatly increased, as compared to the tabulated values [13]. The most uncertain member of the $A = 20$ multiplet is now ^{20}Na , with nearly all of the uncertainty originating from the excitation energy of the $T = 2$ state. The best fit is obtained when a cubic term is included, resulting in $d = 2.8(1.1)$ keV, and $\chi^2 = 3.7$, a result that is an order of magnitude larger than the literature χ^2 value of 0.2 [13]. For the $T = 3/2$, $A = 21$ multiplets, the χ^2 for a quadratic fit have increased to 28 and 9.7 for the $J^\pi = 5/2^+$ and $1/2^+$, respectively, as compared to the literature χ^2 values of 3.0 and 3.5 [13]. The IMME clearly fails in both of the $A = 21$ multiplets. Large cubic terms are required for both

multiplets, with $d = 6.7(13)$ for the $J^\pi = 5/2^+$ multiplet and $d = -4.4(14)$ for the $J^\pi = 1/2^+$ multiplet.

Exploring the impact of isospin-symmetry breaking on nuclear structure is an exciting field of research, as it relates to the symmetries of QCD and their breaking. The sd shell is particularly interesting because it can be accessed by phenomenological and *ab initio* methods. The phenomenological isospin-symmetric USD Hamiltonians [37] generally reproduce data very well throughout the sd shell, but ultimately need to be supplemented with an isospin nonconserving (INC) part [38]. In addition, there are valence-space calculations based on chiral two-nucleon (NN) and three-nucleon ($3N$) forces, without phenomenological adjustments. The resulting sd shell Hamiltonians are inherently isospin asymmetric and have successfully described proton- and neutron-rich systems [39,40], but it is still an open question how well they work in systems with both proton and neutron valence degrees of freedom. Therefore, the current measurements provide valuable new tests of these methods.

We first calculated the IMME in the sd shell with the USDA and USDB isospin-conserving Hamiltonians [37], supplemented with the INC Hamiltonian of Ref. [38]. The results for the $A = 20$ and 21 d and e coefficients are presented in Table II. For $A = 20$, the USDA value for e , which comes from mixing of states with similar energy but different isospin in ^{20}F , ^{20}Ne , and ^{20}Na , agrees with experiment only when e is also included in the IMME fit. Here, the largest mixing comes from a pair of close-lying $J^\pi = 0^+$, $T = 0, 2$ states in ^{20}Ne . With the USDB Hamiltonian, these two states are nearly degenerate, resulting in an uncertainty of the energy of the good isospin states that is too large to give a meaningful result. The calculated d term, on the other hand, comes from mixing in ^{20}F and ^{20}Na . With the USDB, the $J^\pi = 0^+$, $T = 1$ levels in these nuclei are well separated from the $T = 2$ isobaric analog state (IAS), leading to a small energy-mixing shift and, hence, a too small d value.

For the $A = 21$ systems, the USD values of d also do not agree with experiment. The nonzero values come from mixing of the $T = 3/2$ states with close-lying $T = 1/2$ states in ^{21}Ne and ^{21}Na . For instance, the largest shift in the $J^\pi = 5/2^+$ multiplet is due to a $T = 1/2$ state in ^{21}Ne , which for the USDA lies 372 keV below the IAS, instead of the 50 keV necessary to reproduce $d = 6.7$ keV.

TABLE II. Extracted IMME parameters for the $A = 20$ and 21 multiplets. Mass excesses are taken from [30] and excitation energies E_x from [31] and [36], except where noted. Also shown are the d and e coefficients for cubic and quartic fits and the χ^2 values of the fit. Shell model calculation results using the USDA and USDB plus INC interactions are presented.

Nuclide	T_z	ME (g.s.) (keV)	E_x (keV)
$A = 20, J^\pi = 0^+, T = 2$			
^{20}O	+2	3796.17 (89)	0.0
^{20}F	+1	-17.45 (3)	6519.0 (30)
^{20}Ne	0	-7041.9306 (16)	16732.9 (27)
^{20}Na	-1	6850.6 (11)	6524.0 (97) ^a
^{20}Mg	-2	17477.7 (18) ^b	0.0
Ref.	a (keV)	b (keV)	c (keV) χ^2
This work	9689.79 (22)	-3420.57 (50)	236.83 (61) 10.2
Ref. [13]	9693 (2)	-3438 (4)	245 (2) 1.1
	Fit	d (keV)	e (keV) χ^2
	Cubic	2.8 (11)	... 3.7
	Quartic Only	...	0.89 (12) 9.9
	Quartic	5.4 (17)	-3.5 (18) ...
	USDA	-0.1	...
	USDA	...	-1.7
	USDB	-0.1	...
$A = 21, J^\pi = 5/2^+, T = 3/2$			
^{21}F	+3/2	-47.6 (18)	0.0
^{21}Ne	+1/2	-5731.78 (4)	8859.2 (14)
^{21}Na	-1/2	-2184.6 (3)	8976.0 (20)
^{21}Mg	-3/2	10903.85 (74) ^b	0.0
Ref.	a (keV)	b (keV)	c (keV) χ^2
This work	4898.4 (13)	-3651.36 (63)	235.00 (77) 28.0
Ref. [13]	4894 (1)	-3662 (2)	243 (2) 3.0
	Fit	d (keV)	χ^2
	Cubic	6.7 (13)	...
	USDA	-0.3	...
	USDB	0.3	...
$A = 21, J^\pi = 1/2^+, T = 3/2$			
^{21}F	+3/2	-47.6 (18)	279.93 (6)
^{21}Ne	+1/2	-5731.78 (4)	9148.9 (16)
^{21}Na	-1/2	-2184.6 (3)	9217.0 (20)
^{21}Mg	-3/2	10903.85 (74) ^b	200.5 (28) ^c
Ref.	a (keV)	b (keV)	c (keV) χ^2
This work	5170.4 (14)	-3633.6 (10)	220.9 (10) 9.7
Ref. [13]	5171 (10)	-3617 (2)	217 (2) 3.5
	Fit	d (keV)	χ^2
	Cubic	-4.4 (14)	...
	USDA	-1.2	...
	USDB	1.9	...

^a Average of Refs. [31, 33].

^b Present work.

^c Average of Refs. [35, 36].

Experimentally, several $T = 1/2$ states with unidentified spin lie around the IAS [31]. This illustrates the challenge in obtaining accurate calculations capable of describing the new experimental findings.

In addition, we calculated the properties of the $A = 20$ and 21 multiplets from valence-space Hamiltonians constructed within the framework of many-body perturbation theory [41], based on low-momentum [42] NN and $3N$

TABLE III. Experimental and calculated ground-state energies (in MeV) of $^{20,21}\text{Mg}$ with respect to ^{16}O . USDA and USDB results include the INC Hamiltonian discussed in the text.

Nuclide	Exp.	USDA	USDB	$NN + 3N$
^{20}Mg	-6.94	-6.71	-6.83	-6.89
^{21}Mg	-21.59	-21.79	-21.81	-23.18

forces derived from chiral effective field theory [43], without empirical adjustments. These isospin-asymmetric Hamiltonians describe ground- and excited-state properties in neutron-rich oxygen isotopes [39,44,45] and proton-rich $N = 8$ isotones [40]. Here we use the valence-space Hamiltonians of Refs. [39] and Ref. [40] for the neutron-neutron and proton-proton parts, respectively, and include for the first time valence-space proton-neutron interactions. The ground-state energies of $^{20,21}\text{Mg}$ are shown in Table III. The calculated ground-state energy of ^{20}Mg is in very good agreement with experiment, while ^{21}Mg , with one neutron above the closed $N = 8$ shell, is overbound by 1.6 MeV. For the $A = 20$ multiplet, the d coefficient is found to be -18 keV, i.e., giving isospin-symmetry breaking larger than in experiment. As T_z increases, other members of the $A = 21, T = 3/2$ multiplet become less overbound than ^{21}Mg (^{21}F is only 0.8 MeV overbound). This, however, also results in larger cubic terms for the $A = 21$ multiplets ($d = -38$ keV for $A = 21, J^\pi = 5/2^+$). Therefore, the new experimental findings cannot be described with these Hamiltonians, but they nonetheless provide a promising first step towards understanding isospin-symmetry breaking based on electromagnetic and strong interactions.

In summary, we have performed the first direct mass measurement of $^{20,21}\text{Mg}$ using the TITAN Penning trap, making ^{20}Mg the most exotic proton-rich nuclide to be measured in a Penning trap. The new mass of ^{20}Mg is 15 times more precise and deviates from the AME12 value by 3σ , while the new mass of ^{21}Mg agrees with the AME12 but is 22 times more precise. A quadratic fit of the $A = 20$ IMME results in a χ^2 of 10.4, reducing to 3.7 or 9.9 with the inclusion of cubic or quartic terms, respectively. The increased precision of the ^{21}Mg mass now gives, for the $5/2^+$ multiplet, $\chi^2 = 28$ with a quadratic IMME, making the $A = 20$ and 21 multiplets new members of the sd shell to present strong deviations from the quadratic form of the IMME. In both cases shell-model calculations are presently unable to predict the required cubic d coefficients. Further Penning trap measurements of members of other multiplets will be valuable to better test some of the proposed mechanisms for cubic and quartic terms. With the on-line use of the IG-LIS, such exotic nuclei will be available contaminant free, paving the way for new experiments far from stability.

This work was supported by the Natural Sciences and Engineering Research Council of Canada (NSERC).

A. T. G. acknowledges support from the NSERC CGS-D program and A. L. from the DFG under Grant No. FR601/3-1. This work was also supported by the BMBF under Contract No. 06DA70471, the DFG through Grant No. SFB 634, the Helmholtz Association through the Helmholtz Alliance Program, Contract No. HA216/EMMI “Extremes of Density and Temperature: Cosmic Matter in the Laboratory.” Computations were performed with an allocation of advanced computing resources at the Jülich Supercomputing Center. We acknowledge support from NSF Grant No. PHY-1068217 and the NSF REU program at MSU.

*agallant@triumf.ca

[†]Present address: TRIUMF, 4004 Wesbrook Mall, Vancouver, British Columbia, V6T 2A3 Canada.

^{*}Present address: Rare Isotope Science Project (RISP), Institute for Basic Science, Daejeon 305-811, Republic of Korea.

- [1] Y. Blumenfeld, T. Nilsson, and P. Van Duppen, *Phys. Scr.* **T152**, 014023 (2013).
- [2] K. Blaum, *Phys. Rep.* **425**, 1 (2006).
- [3] R. N. Wolf *et al.*, *Phys. Rev. Lett.* **110**, 041101 (2013).
- [4] J. Van Schelt *et al.*, *Phys. Rev. Lett.* **111**, 061102 (2013).
- [5] A. T. Gallant *et al.*, *Phys. Rev. Lett.* **109**, 032506 (2012).
- [6] F. Wienholtz *et al.*, *Nature (London)* **498**, 346 (2013).
- [7] D. Steppenbeck *et al.*, *Nature (London)* **502**, 207 (2013).
- [8] H.-W. Hammer, A. Nogga, and A. Schwenk, *Rev. Mod. Phys.* **85**, 197 (2013).
- [9] K. Blaum, J. Dilling, and W. Nörtershäuser, *Phys. Scr.* **T152**, 014017 (2013).
- [10] Y. H. Zhang *et al.*, *Phys. Rev. Lett.* **109**, 102501 (2012).
- [11] M. Brodeur, T. Brunner, S. Ettenauer, A. Lapierre, R. Ringle, B. A. Brown, D. Lunney, and J. Dilling, *Phys. Rev. Lett.* **108**, 212501 (2012).
- [12] C. Yazidjian *et al.*, *Phys. Rev. C* **76**, 024308 (2007).
- [13] Y. H. Lam, B. Blank, N. A. Smirnova, J. B. Bueb, and M. S. Antony, *At. Data Nucl. Data Tables* **99**, 680 (2013).
- [14] R. J. Charity *et al.*, *Phys. Rev. C* **84**, 051308(R) (2011).
- [15] A. A. Kwiatkowski *et al.*, *Phys. Rev. C* **80**, 051302(R) (2009).
- [16] A. Kankainen *et al.*, *Phys. Rev. C* **82**, 052501(R) (2010).
- [17] G. Savard, St. Becker, G. Bollen, H.-J. Kluge, R. B. Moore, Th. Otto, L. Schweikhard, H. Stolzenberg, and U. Wiess, *Phys. Lett. A* **158**, 247 (1991).
- [18] H. Wollnik and M. Przewłoka, *Int. J. Mass Spectrom. Ion Process.* **96**, 267 (1990).
- [19] R. N. Wolf *et al.*, *Nucl. Instrum. Methods Phys. Res., Sect. A* **686**, 82 (2012).
- [20] D. A. Fink *et al.*, *Nucl. Instrum. Methods Phys. Res., Sect. B* **317**, 417 (2013).
- [21] K. Blaum, C. Geppert, H.-J. Kluge, M. Mukherjee, S. Schwarz, and K. Wendt, *Nucl. Instrum. Methods Phys. Res., Sect. B* **204**, 331 (2003).
- [22] S. Raeder, H. Heggen, J. Lassen, F. Ames, D. Bishop, P. Bricault, P. Kunz, A. Mjøs, and A. Teigelhöfer, *Rev. Sci. Instrum.* **85**, 033309 (2014).
- [23] J. Dilling *et al.*, *Int. J. Mass Spectrom.* **251**, 198 (2006).
- [24] T. Brunner *et al.*, *Nucl. Instrum. Methods Phys. Res., Sect. A* **676**, 32 (2012).
- [25] A. Lapierre *et al.*, *Nucl. Instrum. Methods Phys. Res., Sect. A* **624**, 54 (2010).
- [26] M. Brodeur *et al.*, *Int. J. Mass Spectrom.* **310**, 20 (2012).
- [27] M. König, G. Bollen, H.-J. Kluge, T. Otto, and J. Szerypo, *Int. J. Mass Spectrom. Ion Process.* **142**, 95 (1995).
- [28] S. Ettenauer *et al.*, *Phys. Rev. C* **81**, 024314 (2010).
- [29] M. Brodeur *et al.*, *Phys. Rev. C* **80**, 044318 (2009).
- [30] M. Wang, G. Audi, A. H. Wapstra, F. G. Kondev, M. MacCormick, X. Xu, and B. Pfeiffer, *Chin. Phys. C* **36**, 1603 (2012).
- [31] Evaluated Nuclear Structure Data File, <http://www.nndc.bnl.gov/ensdf/>.
- [32] C. Wrede *et al.*, *Phys. Rev. C* **81**, 055503 (2010).
- [33] W. Geithner *et al.*, *Phys. Rev. Lett.* **101**, 252502 (2008).
- [34] J. P. Wallace *et al.*, *Phys. Lett. B* **712**, 59 (2012).
- [35] C. Aa. Diget *et al.*, *Phys. Rev. C* **77**, 064309 (2008).
- [36] R. B. Firestone, *Nucl. Data Sheets* **103**, 269 (2004).
- [37] B. A. Brown and W. A. Richter, *Phys. Rev. C* **74**, 034315 (2006).
- [38] W. E. Ormand and B. A. Brown, *Nucl. Phys.* **A491**, 1 (1989).
- [39] J. D. Holt, J. Menéndez, and A. Schwenk, *Eur. Phys. J. A* **49**, 39 (2013).
- [40] J. D. Holt, J. Menéndez, and A. Schwenk, *Phys. Rev. Lett.* **110**, 022502 (2013).
- [41] M. Hjorth-Jensen, T. T. S. Kuo, and E. Osnes, *Phys. Rep.* **261**, 125 (1995).
- [42] S. K. Bogner, R. J. Furnstahl, and A. Schwenk, *Prog. Part. Nucl. Phys.* **65**, 94 (2010).
- [43] E. Epelbaum, H.-W. Hammer, and U.-G. Meißner, *Rev. Mod. Phys.* **81**, 1773 (2009).
- [44] T. Otsuka, T. Suzuki, J. D. Holt, A. Schwenk, and Y. Akaishi, *Phys. Rev. Lett.* **105**, 032501 (2010).
- [45] C. Caesar *et al.*, *Phys. Rev. C* **88**, 034313 (2013).